Supporting Information

Noble-metal-free Ni–W–O derived catalysts for high-capacity hydrogen production from hydrazine monohydrate

Qing Shi,[†] Deng-Xue Zhang,[†] Hui Yin,[†] Yu-Ping Qiu,[†] Liang-Liang Zhou,[†] Chen Chen,[†] Hui Wu,[‡] and Ping Wang[†*]

[†] School of Materials Science and Engineering, Key Laboratory of Advanced Energy Storage Materials of Guangdong Province, South China University of Technology, Guangzhou 510641, P.R. China

[‡] NIST Center for Neutron Research, National Institute of Standards and Technology, Gaithersburg, Maryland 20899-6102, United States

[*] Corresponding author. Tel: +86 20 3938 0583

E-mail address: mspwang@scut.edu.cn (P. Wang)

Number of pages: 15

Number of figures: 11

Number of tables: 1

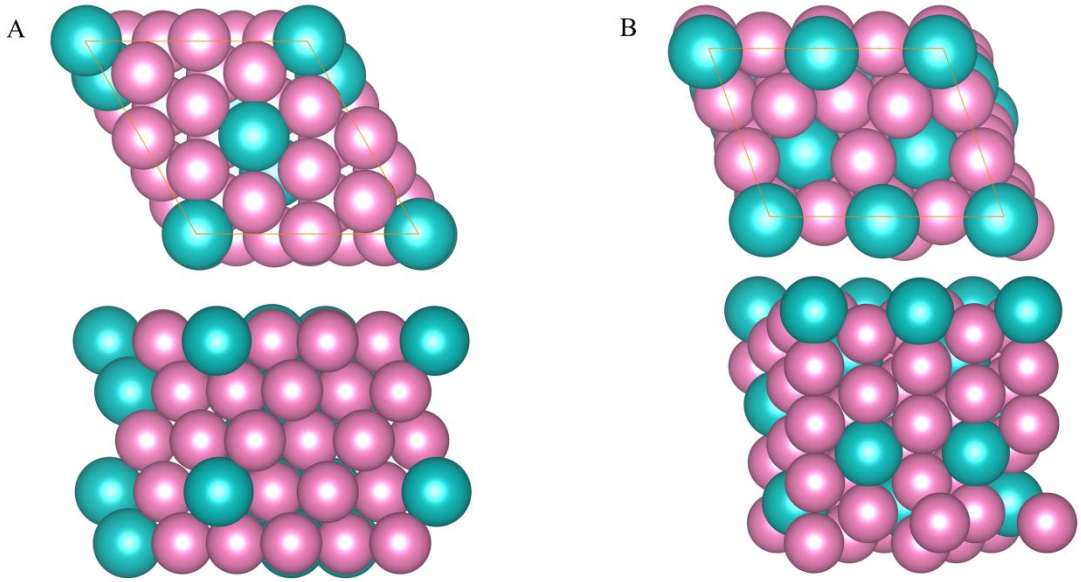

Figure S1. Top and front views of the models of (A) $Ni_{17}W_3$(111)-plane, (B) Ni_4W (211)-plane. The pink and cyan balls denote Ni and W atoms, respectively.

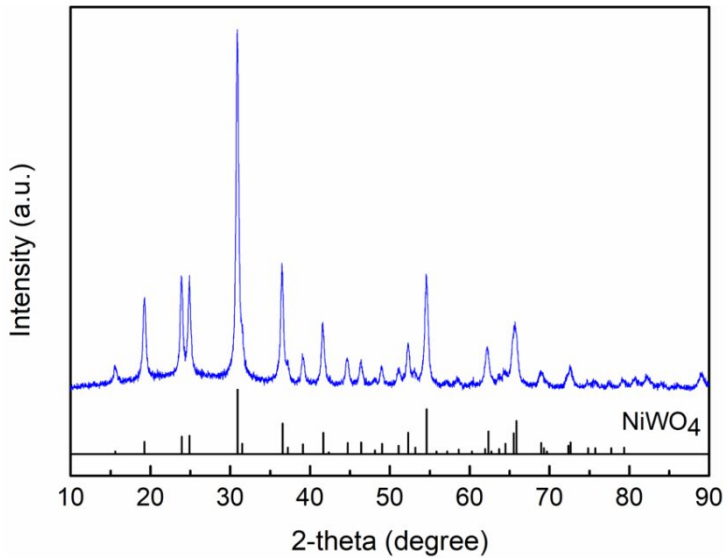

Figure S2. XRD pattern of 450 ^{o}C-annealed sample under air atmosphere.

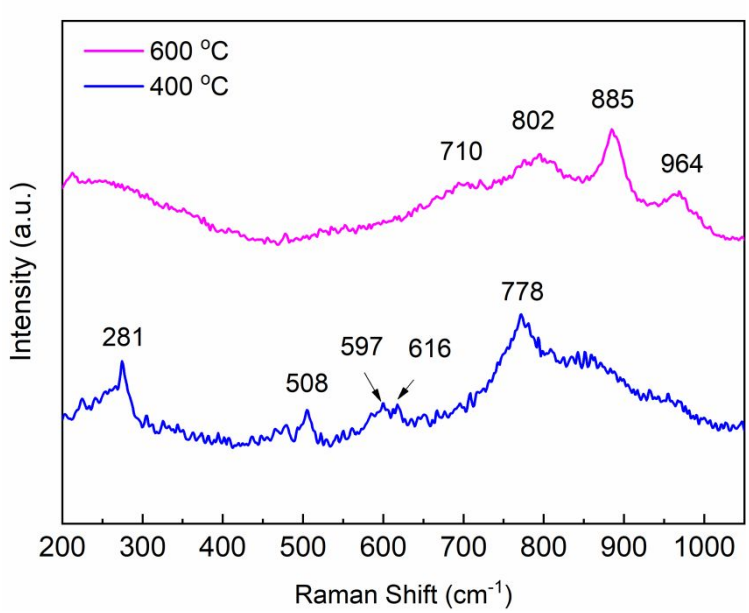

Figure S3. Raman spectra of the 400 °C- and 600 °C-reduced samples. For the 400 °C-reduced sample, the bands at 778, 616, 597, 508 and 281 cm^{-1} can be safely assigned to the characteristic modes of WO_2.[1,2] For the 600 °C-reduced sample, the bands at 710, 802 and 964 cm^{-1} should be ascribed to the vibration modes of WO_3. Specifically, the bands at 710 and 802 cm^{-1} correspond to the symmetric stretching and bending modes of W-O, and the band at 964 cm^{-1} to the stretching mode of terminal W=O bonds.[3,4] The band at 885 cm^{-1} was ascribed to the symmetric stretching mode of terminal W=O bonds of the residual $NiWO_4$ phase.[5,6]

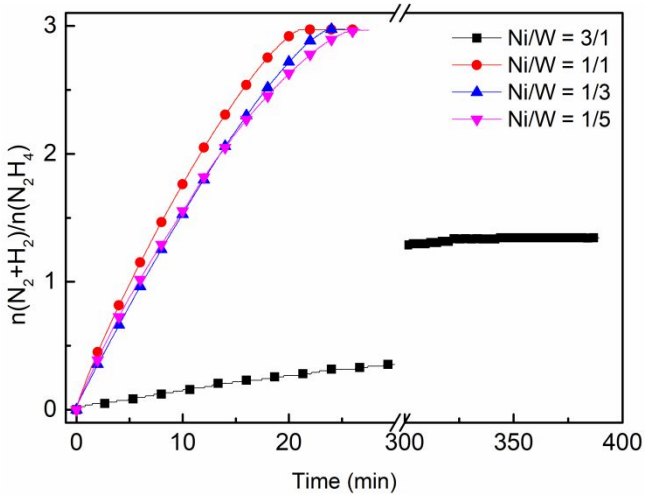

Figure S4. The kinetic curves of $N_2H_4 \cdot H_2O$ decomposition over the reduced catalysts with the different molar ratios of Ni to W precursors at 400 °C H_2 atmosphere. The catalytic decomposition of $N_2H_4 \cdot H_2O$ was conducted in a solution (2 mL) of 0.5 M $N_2H_4 \cdot H_2O$ + 2.0 M NaOH at 50 °C.

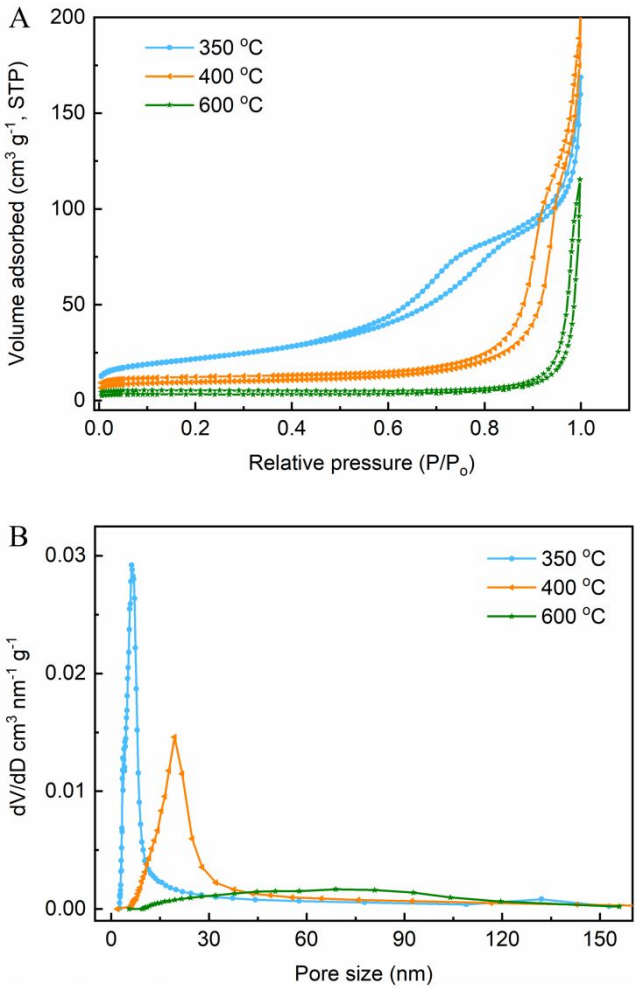

Figure S5. (A) N_2 sorption isotherms and (B) the corresponding pore size distribution curves for the samples reduced at various temperatures.

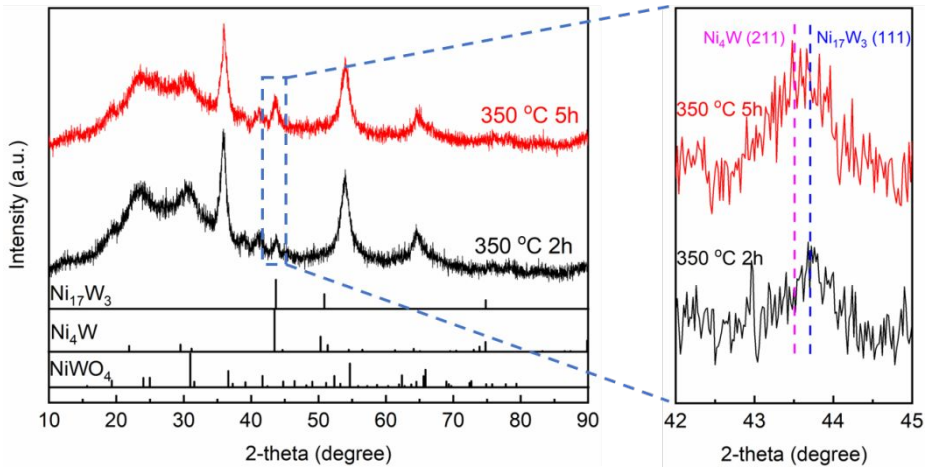

Figure S6. XRD patterns of the nanocomposite samples annealed at 350 °C for different time.

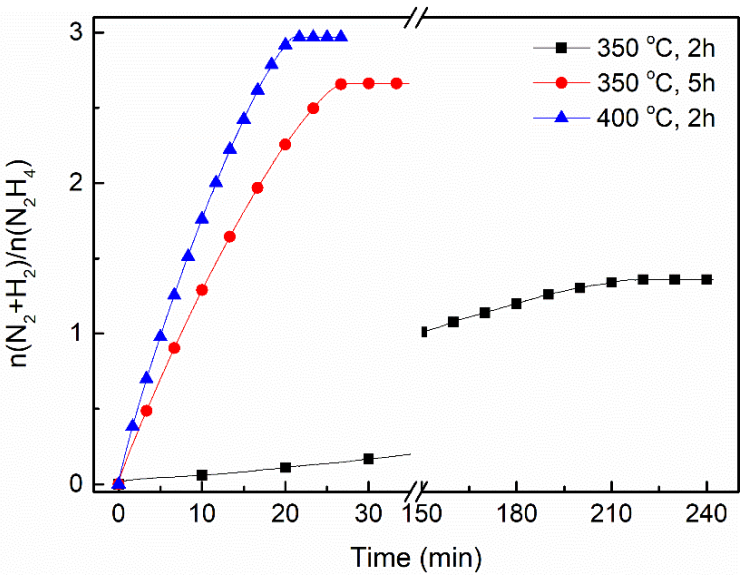

Figure S7. The kinetic curves of $N_2H_4 \cdot H_2O$ decomposition over the reduced catalysts at different temperatures or annealing time. The catalytic decomposition of $N_2H_4 \cdot H_2O$ was conducted in a solution (2 mL) of 0.5 M $N_2H_4 \cdot H_2O$ + 2.0 M NaOH at 50 °C.

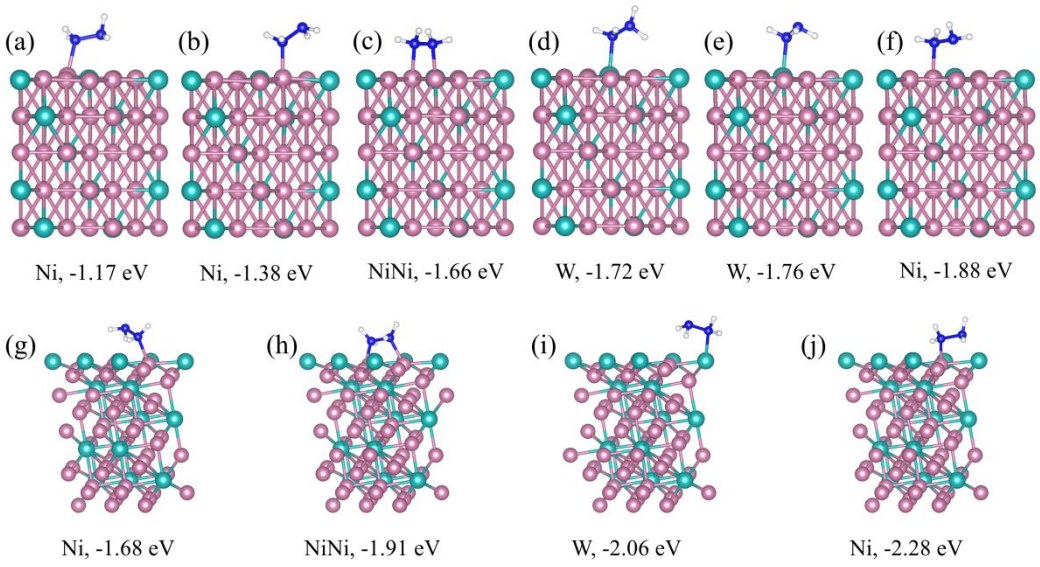

Figure S8. Possible adsorption conformations of N_2H_4 on (a-f) $Ni_{17}W_3$ (111) and (g-j) Ni_4W (211) surfaces and the corresponding adsorption energies. Same adsorption conformation of N_2H_4 can be obtained from different initial conformations after optimization, for example, (i) can be obtained from both anti and gauche configurations of N_2H_4 adsorbed on W atom of Ni_4W (211) surface.

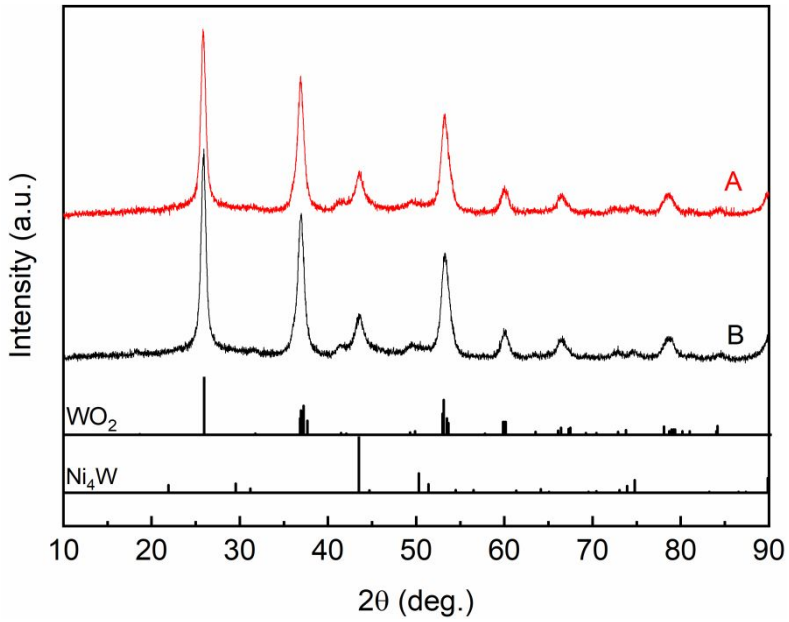

Figure S9. XRD patterns of 400 °C-reduced catalyst sample before (A) and after (B) the stability test.

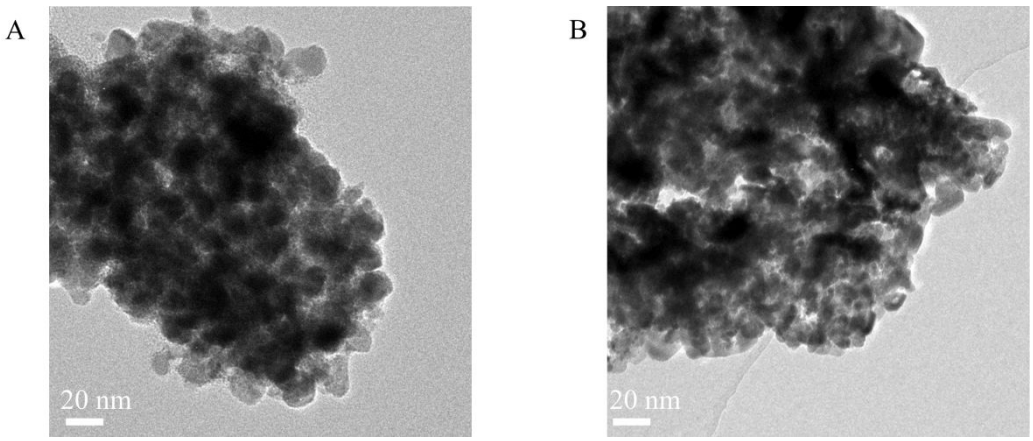

Figure S10. TEM images of the 400 °C-reduced catalyst sample before (A) and after (B) the stability test.

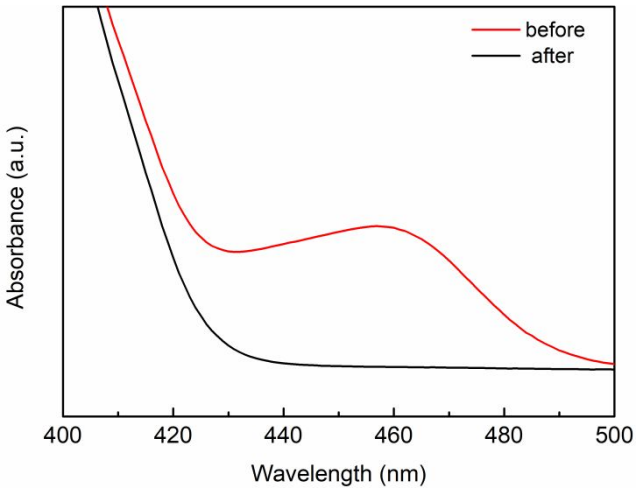

Figure S11. UV–vis spectra of hydrous hydrazine solution before and after the catalytic decomposition reaction over the 400 ^{o}C-reduced catalyst sample.

Table S1. Comparison of catalytic performance of the noble-metal-free catalysts towards hydrogen generation from $N_2H_4 \cdot H_2O$.

Catalyst	Reaction rate (h^{-1})	Selectivity (%)	Temperature (^oC)	Activity attenuation[a] (%)	Reference
$NiMoB\text{-}La(OH)_3$	13.3	100	50	52	7
$Ni\text{-}Al_2O_3\text{-}HT$	2.0	93	50	40	8
$Ni_{10}Mo/Ni\text{-}Mo\text{-}O$	54.5	97	50	<5	9
$NiCO/NiO\text{-}CoO_x$	5.49	99	25	30	10
$2D\ NiFe/CeO_2$	5.73	99	50	35	11
$6\ wt\%Ni/CeO_2$	34.0	100	50	15[b]	12
Ni nanofiber	6.9	100	60	24[c]	13
$NiFe/CeZrO_2$	24.7	100	50	48[c]	14
$Ni_4W/WO_2/NiWO_4$	33	99	50	<5	This work

[a] Activity attenuation after 10 cyclic usage; [b] 3 cyclic usage; [c] 5 cyclic usage.

References

(1) Liu, F.; Li, L.; Mo, F.; etc. A Catalyzed-Growth route to directly form micropatterned WO_2 and WO_3 nanowire arrays with excellent field emission behaviors at low temperature. *Cryst. Growth Des.* **2010**, *10*, 5193–5199.

(2) Frey, G. L.; Rothschild, A.; Sloan, J.; etc. Investigations of nonstoichiometric tungsten oxide nanoparticles. *J. Solid State Chem.* **2001**, *162*, 300–313.

(3) Fang, G.; Liu, Z.; Yao, K. L. Fabrication and characterization of electrochromic nanocrystalline WO_3/Si(111) thin films for infrared emittance modulation applications. *J. Phys. D: Appl. Phys.* **2001**, *34*, 2260–2266.

(4) Kim, D. S.; Ostromecki, M.; Wachs, I. E. Preparation and characterization of WO_3/SiO_2 catalysts. *Catal. Lett.* **1995**, *33*, 209–215.

(5) Xing, X.; Wang, J.; Reduced graphene oxide incorporated $NiWO_4$ for high-performance energy storage. *J Mater Sci: Mater Electron* **2016**, *27* (11), 11613–11622.

(6) Xu, X.; Pei, L.; Yang, Y.; etc. Facile synthesis of $NiWO_4$/reduced graphene oxide nanocomposite with excellent capacitive performance for supercapacitors. *J. Alloys Compd.* **2016**, *654*, 23–31.

(7) Zhang, J.; Kang, Q.; Yang, Z.; etc. A cost-effective NiMoB-$La(OH)_3$ catalyst for hydrogen generation from decomposition of alkaline hydrous hydrazine solution. *J. Mater. Chem. A* **2013**, *1* (38), 11623–11628.

(8) He, L.; Huang, Y.; Wang, A.; etc. A noble-metal-free catalyst derived from Ni-Al hydrotalcite for hydrogen generation from $N_2H_4 \cdot H_2O$ decomposition. *Angew. Chem. Int. Ed.* **2012**, *51* (25), 6191–6194.

(9) Qiu, Y. P.; Cao, G. X.; Wen, H.; etc. High-capacity hydrogen generation from hydrazine monohydrate using a noble-metal-free $Ni_{10}Mo$/Ni-Mo-O nanocatalyst. *Int. J. Hydrogen Energy*, **2019**, *44* (29), 15110–15117.

(10) Wu, D.; Wen, M.; Lin, X.; etc. A NiCo/NiO–CoO_x ultrathin layered catalyst with strong basic sites for high-performance H_2 generation from hydrous hydrazine. *J. Mater. Chem. A*, **2016**, *4* (17), 6595–6602.

(11) Wu, D.; Wen, M.; Gu, C.; etc. 2D NiFe/CeO_2 basic-site-enhanced catalyst via in-situ topotactic reduction for selectively catalyzing the H_2 generation from $N_2H_4 \cdot H_2O$. *ACS Appl. Mater. Interfaces* **2017**, *9* (19), 16103–16108.

(12) Kang, W.; Varma, A. Hydrogen generation from hydrous hydrazine over Ni/CeO_2 catalysts prepared by solution combustion synthesis. *Appl. Catal. B* **2018**, *220*, 409–416.

(13) Fu, Q.; Yang, P.; Wang, J.; etc. In situ synthesis of Ni nanofibers via vacuum thermal reduction and their efficient catalytic properties for hydrogen generation. *J. Mater. Chem. A* **2018**, *6* (24), 11370–11376.

(14) Zou, H.; Yao, Q.; Huang, M.; etc. Noble-metal-free NiFe nanoparticles immobilized on nano $CeZrO_2$ solid solutions for highly efficient hydrogen production from hydrous hydrazine. *Sustainable Energy Fuels*, **2019**, *3*, 3071–3077.